Contact Angle, Wettability and Adhesion, Vol. 4, pp. 43–59
Ed. K.L. Mittal

The detailed structure of a perturbed wetting triple line on modified PTFE

CATHERINE COMBELLAS,[1] ADRIEN FUCHS,[1] FRÉDÉRIC KANOUFI,[1,*] and MARTIN E. R. SHANAHAN[2]

[1]*Laboratoire Environnement et Chimie Analytique, Ecole Supérieure de Physique et Chimie, Industrielles, 10 rue Vauquelin, 75231 Paris Cedex 05, France*
[2]*Centre des Matériaux de Grande Diffusion, Ecole des Mines d'Alès, 6 avenue de Clavières, 30319 Alès Cedex, France*

Abstract—The essential form of an initially straight wetting triple line perturbed by the presence of a (higher surface free energy) "defect" on the solid surface has been recognised for a long time, and it corresponds to a logarithmically decaying form. However, less attention has been paid to the behaviour of the triple line within the domain of the defect. This was actually studied a few years ago from a theoretical viewpoint, leading to the prediction of an inversion of curvature. Recent experimental work has been concerned with the electrochemical treatment of PTFE, leading to small etched areas of higher wettability with typical widths of 100–300 μm. Wetting experiments have been carried out on such solids and the results confirm the general conclusion of inverted curvature of the triple line in the treated zones. However, the "excess wettability" in the treated zones, as evaluated experimentally, was found to be greater than predicted theoretically. Possible causes are discussed.

Keywords: Defect; electrochemical treatment; fine structure; surface modification; wetting line; PTFE.

1. INTRODUCTION

Surface treatments of polymers have many uses, such as the enhancement of aesthetic properties (optical or tactile feeling), in increasing wear resistance, in decreasing friction coefficient, or, on the other hand, in increasing adhesion when bonding the polymer in question to another material. Fluoropolymers, in particular, have innately low surface free energies (or tensions), which is a useful feature when low friction is required but is a bane for bonding.

Electrochemical techniques have been developed to modify the surface free energy and, therefore, the wettability of polymeric solid surfaces. Scanning Electro-

*To whom correspondence should be addressed. Tel.: (33-1) 4079-4526; Fax: (33-1) 4079-4425; e-mail: frederic.kanoufi@espci.fr

chemical Microscopy (SECM) is one of these promising techniques [1]. Therefore, we have carried out surface treatment of poly(tetrafluoroethylene) (PTFE) using SECM. This method is capable of producing very small areas (typical dimensions: 100 μm) of treated surface presenting higher values of surface free energy than their surrounding zones.

Classical wetting techniques, such as the measurement of contact angles of sessile drops of probe liquids, are very sensitive to variations in surface properties, yet are only applicable to regions of typical dimensions of 1 mm or greater. As a consequence, such an approach is precluded as a method for the characterization of the small SECM-treated surface areas mentioned above.

However, in recent years developments in wetting theory have considered the deformed shape of a wetting triple line when in the proximity of a "defect", or small region presenting either a higher or a lower (higher in the present case) surface free energy and, therefore, wettability, as defined by contact angle [2–6], than the neighboring solid region. The "defect" can have dimensions of about 100 μm, and yet produce noticeable and quantifiable perturbations to the triple line shape. Thus, the analysis of observed distorted wetting fronts lends itself well to the characterization of solid surfaces modified on the size scale discussed above.

In this work we have compared the expression for a deformed triple line, obtained recently, to experimental data and have extended our analysis to the case of diffuse defects that are generally obtained by chemical or optical techniques. Indeed, chemical or optical techniques rarely produce local surface modification with sharp boundaries, but rather generate modifications whose edges are diffuse. Thus, as a continuation of earlier work [7], we consider here the wetting properties of PTFE surface, locally marked by higher surface free energy regions of small dimensions, obtained by targeted chemical modification.

2. THEORETICAL EQUATIONS OF TRIPLE LINE

The triple wetting line for the liquid/homogeneous solid/vapour (V) system obeys Young's equation at equilibrium [8]:

$$\gamma_{SV} = \gamma_{SL} + \gamma \cos\theta \tag{1}$$

where γ_{SV}, γ_{SL} and γ are, respectively, solid/vapour, solid/liquid and liquid/vapour interfacial tensions, and θ is the characteristic equilibrium contact angle of the system. However, if the solid surface presents a heterogeneity also called "defect" (and, thus, is no longer entirely homogeneous) in the immediate vicinity of the contact line, which we shall assume to represent an increase in wettability, or a decrease in local contact angle, a deformation of the triple line will occur: the liquid front will protrude to cover at least part of the defect and gently return to its unperturbed level, following a logarithmic law, as distance from the defect increases (see Fig. 1). The triple line is then "pinned" on the defect and yet

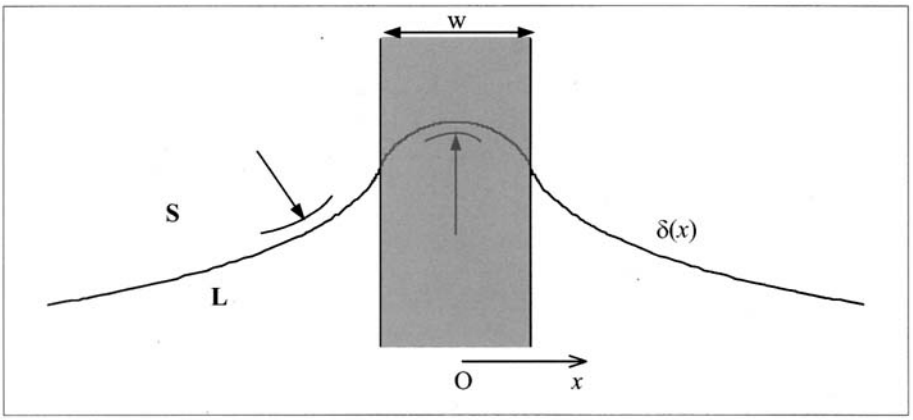

Figure 1. Schematic representation of liquid/solid/vapour triple line perturbed by solid surface energy heterogeneity of width w.

is "pulled" by the far field of the unperturbed contact line. This "elasticity" effect of the triple line has been studied both theoretically and experimentally by several workers [2, 4–6, 9]. Using the nomenclature of Fig. 1, the basic form of the triple line can be described by the protrusion distance, $\delta(x)$, as a function of distance $|x|$ from the centre of the defect [2].

$$\delta(x) \approx \frac{f}{\pi\gamma\theta^2} \ln\frac{r_o}{|x|}, \quad |x| > \frac{w}{2} \tag{2}$$

where f is the "pull force" of the heterogeneity, w is heterogeneity width and r_0 is a macroscopic cut-off distance. θ represents the equilibrium contact angle on the homogeneous solid, outside of the defect. The pull force is defined as the force due to variation in the surface free energy ε at the heterogeneity:

$$\varepsilon(x,y) = (\tilde{\gamma}_{SV}(x,y) - \tilde{\gamma}_{SL}(x,y)) - (\gamma_{SV} - \gamma_{SL}) = \gamma(\cos\tilde{\theta}(x,y) - \cos\theta) \tag{3}$$

where $\tilde{\gamma}_{SV}$, $\tilde{\gamma}_{SL}$ and $\tilde{\theta}$ refer to interfacial tensions and contact angle on the heterogeneous material, $|x| < w/2$, and γ_{SV}, γ_{SL} and θ are the same quantities for the virgin homogeneous solid, $|x| > w/2$.

The pull force, f, is then expressed as:

$$f = \int \varepsilon(x, \delta(x))\mathrm{d}x \tag{4}$$

Equation (2) was derived using energy minimization principles and Fourier transform methods, assuming an initially straight triple line [2].

In a different, but related, approach, the meniscus shape of a slightly deformed axisymmetric drop, of radius r_0, was derived using the Fourier series analysis [6]. Briefly, in cylindrical coordinates (r is the radial coordinate and φ the azimuthal one), the local deformation of the contact line is given by:

$$\delta(\varphi) = \frac{r_0}{\gamma\theta^2}\left\{-B_0(r_0)/2 + \sum_{n=2}^{\infty}\frac{A_n(r_0)\sin n\varphi + B_n(r_0)\cos n\varphi}{n-1}\right\} \tag{5}$$

where θ is the unperturbed contact angle and the coefficients A_i and B_i are obtained from the Fourier form of ε near the drop periphery:

$$\varepsilon(r_0,\varphi) = B_0(r_0)/2 + \sum_{m=1}^{\infty} A_m(r_0)\sin m\varphi + B_m(r_0)\cos m\varphi \tag{6}$$

This analysis leads to a considerably more complicated expression for $\delta(x)$, but intrinsically also allows to account for the behaviour within the defect, $|x| < w/2$, which equation (2) cannot.

2.1. Square profile (sharp stripe defect)

Let us consider a single heterogeneity near the periphery of the drop such that ε is expressed by a square function:

$$\varepsilon(r_0,\varphi) = \begin{cases} 0 & -\pi < \varphi < -\chi \\ \varepsilon_0 & -\chi < \varphi < \chi \\ 0 & \chi < \varphi < \pi \end{cases} \tag{7}$$

where ε_0 corresponds to the gain in surface free energy introduced by the heterogeneity.

The Fourier coefficients obtained from (7) inserted in (5) lead to a complicated, yet straightforward, expression for the contact line deformation:

$$\delta(\varphi) = \frac{r_0\varepsilon_0}{\pi\gamma\theta^2}\left\{-\chi + 2\sum_{n=1}^{\infty}\frac{\sin(n\chi)}{n(n-1)}\cos(n\varphi)\right\} \tag{8}$$

It may be simplified with standard trigonometric rules by using the following identities:

$$\sum_{n>0}\frac{\cos(n\alpha)}{n} = \ln\left(\frac{1}{2\sin\frac{\alpha}{2}}\right) \tag{9}$$

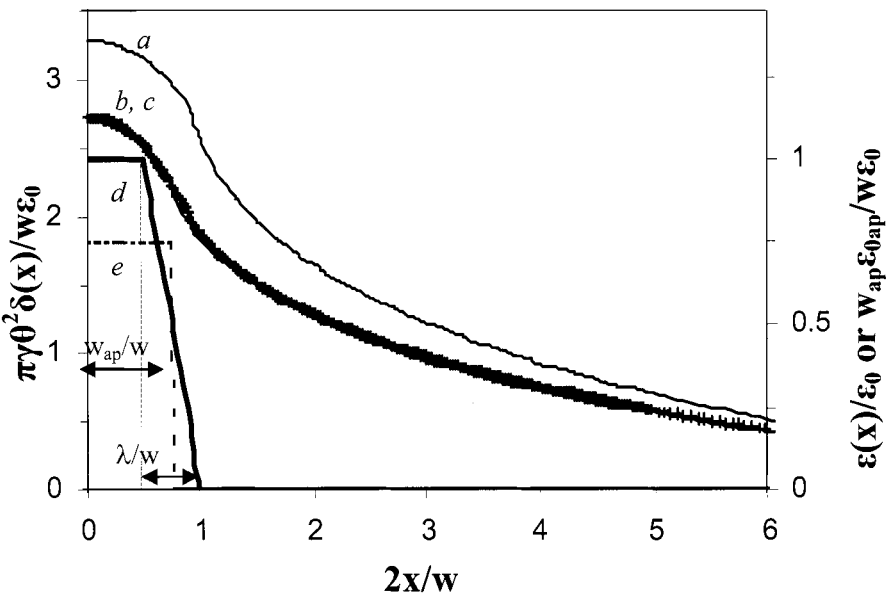

Figure 2. (a, b, c) Triple line profiles for different defect types. (a) Triple line deformation according to equation (11) for a sharp defect of width w and strength $w\varepsilon_0$. (b) Triple line deformation according to equation (15) for the diffuse defect profile (d), with $\lambda = 0.25$ w and strength $w\varepsilon_0$. (c) best fit of the front (b) by the sharp defect model according to equation (11) with the values of $w_{ap} = 0.75$ w and $w_{ap}\varepsilon_{0ap} = 0.75\ w\varepsilon_0$. On the left axis, unit for the triple line profiles (a, b, c) obtained for $w\varepsilon_0/\gamma\theta^2=1$. On the right axis, unit for the defect surface free energy profiles (d, e).

$$\sum_{n>0} \frac{\sin(n\alpha)}{n} = \frac{1}{2}(\pi - \alpha) \tag{10}$$

and allowing the radius of the curved triple line of the sessile drop, r_0, to tend to infinity [10], we obtain the following basic equation for the perturbed contact line:

$$\delta(x) = \frac{w\varepsilon_0}{2\pi\gamma\theta^2}\left\{(x^*+1)\ln\left(\frac{1}{x^*+1}\right) - (x^*-1)\ln\left(\frac{1}{|x^*-1|}\right)\right\} + C \tag{11}$$

where $x^* = 2|x|/w$ and C is a constant. The triple line deformation obtained from equation (11) for a defect of width w and strength $f = w\varepsilon_0$ with $w\varepsilon_0/\gamma\theta^2 = 1$ is shown schematically in Fig. 1 and as curve a in Fig. 2.

An interesting consequence of equation (11) is that the triple line is predicted to be concave, with respect to the liquid phase, outside of the zone occupied by the

defect, in accordance with equation (2) and yet is convex within the defect. Equation (2) does not consider the latter aspect.

2.2. *Trapezoidal profile (diffuse defect)*

Using the same strategy, one may similarly derive the contact line deformation for a stripe of a diffuse defect of total width w. In this case, ε is described by a trapezoidal function:

$$\varepsilon(r_0,\varphi)=\begin{cases}0 & -\pi<\varphi<-\chi_2-\chi_1\\ \varepsilon_0(\varphi+\chi_2+\chi_1)/\chi_2 & -\chi_2-\chi_1<\varphi<-\chi_1\\ \varepsilon_0 & -\chi_1<\varphi<\chi_1\\ \varepsilon_0(-\varphi+\chi_2+\chi_1)/\chi_2 & \chi_1<\varphi<\chi_2+\chi_1\\ 0 & \chi_2+\chi_1<\varphi<\pi\end{cases} \tag{12}$$

where the linear decrease (see Fig. 2, curve d) corresponds, for instance, to mixing of the low and high surface free energy materials along a diffusion length, $\lambda \approx \chi_2 r_0$. Typically, in the local chemical transformation of a low surface energy into a high surface energy material by a source of a chemical species, λ is the so-called reaction length where the chemical substance is depleted due to its reaction with the surface.

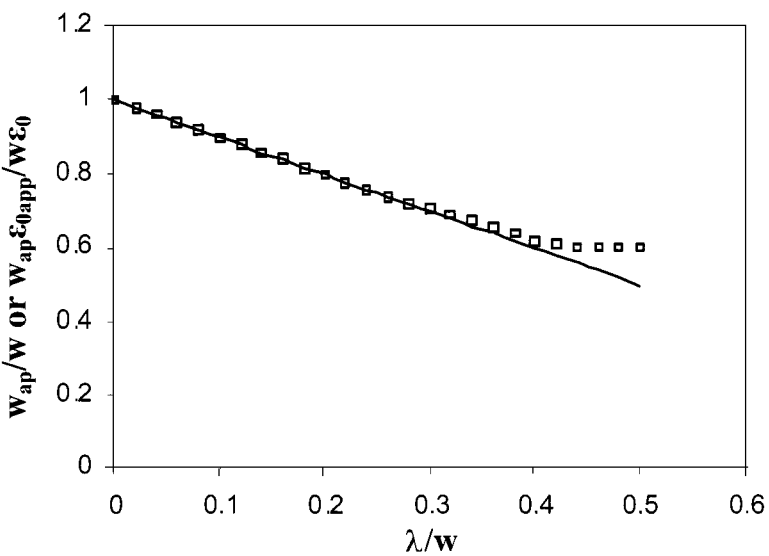

Figure 3. Values of the apparent sharp defect width (□), w_{ap}, and strength (⁻), $w_{ap}\varepsilon_{0ap}$, required in the sharp defect model of triple line front deformation according to equation (11) to fit the triple line front deformation by a diffuse defect of width w and strength $w\varepsilon_0$ according to equation (15).

From the Fourier series corresponding to this surface free energy profile, the theoretical triple line profile may be easily obtained as a Fourier series expression:

$$\delta(\varphi) = \frac{r_0\varepsilon_0}{\pi\gamma\theta^2}\left\{-\chi_1 - \frac{\chi_2}{2} - \frac{2}{\chi_2}\sum_{n=1}^{\infty}\frac{\cos(n(\chi_1+\chi_2)) - \cos(n\chi_1)}{n^2(n-1)}\cos(n\varphi)\right\} \quad (13)$$

It is converted using trigonometric transformations (9), (10) and (14)

$$\sum_{n>0}\frac{\cos(n\alpha)}{n^2} = \frac{1}{6} + \frac{\alpha^2}{4} - \pi\frac{|\alpha|}{2} \quad (14)$$

into the following equation (when allowing r_0 to tend to infinity):

$$\delta(x) = \frac{w\varepsilon_0}{2\pi\gamma\theta^2}\left\{\frac{(1+x^*)^2}{2\lambda^*}\ln\left(\frac{1}{x^*+1}\right) + \frac{(1-x^*)^2}{2\lambda^*}\ln\left(\frac{1}{|1-x^*|}\right)\right.$$

$$\left. - \frac{(1-\lambda^*+x^*)^2}{2\lambda^*}\ln\left(\frac{1}{1-\lambda^*+x^*}\right) - \frac{(1-\lambda^*-x^*)^2}{2\lambda^*}\ln\left(\frac{1}{|1-\lambda^*-x^*|}\right)\right\} + C' \quad (15)$$

with $\lambda^*=2\lambda/w$.

The surface free energy profile $\varepsilon(x)$ obtained by extension of $\varepsilon(r,\varphi)$ to infinity and the corresponding theoretical triple line profiles (15) are presented in Fig. 2 (curves b and d, respectively) in the case of $\lambda = 0.25$ w.

Equation (15) has been computed for a trapezoidal-shaped stripe defect (diffuse defect) of total width w, for the special case of $\lambda = 0.25$ w and is compared to equation (11) for the sharp-defect case of the same width w. As expected, a diffuse defect of width w exerts a lower pinning force on the liquid front than a sharp defect of the same width. Moreover, for the whole range of diffuse lengths, λ, the triple line front of the diffuse defect may be satisfactorily fitted (with less than 5% error) by the sharp defect for which the stripe defect has an apparent surface free energy equal to ε_{0ap} and an apparent size defect w_{ap}. This situation is illustrated in Fig. 2, where the diffuse defect ($\lambda = 0.25$ w) defined by the excess surface free energy given in curve d deforms the triple line front (curves b and c) as much as a sharp defect of apparent width $w_{ap} = 0.75$ w and apparent strength $w_{ap}\varepsilon_{0ap} = 0.75\ w\varepsilon_0$ (see curve e). The variations of the best values of w_{ap} and $w_{ap}\varepsilon_{app}$ for different diffuse lengths λ are presented in Fig. 3. For $\lambda < 0.4$w, we find $w_{ap} \approx w-\lambda$ within 5% error and $w_{ap}\varepsilon_{0ap} = f = w\langle\varepsilon\rangle = (w-\lambda)\varepsilon_0$ where $\langle\varepsilon\rangle$ is the mean surface free energy of the diffuse defect over the whole defect length.

From a practical point of view, the diffusive part of a defect may not be observable. From the fitting of the triple line deformation to the sharp defect model, one obtains the apparent width of the defect $w_{ap} = w-\lambda$. This value can be compared to the observed value of the defect width, w_{exp}. If $w_{exp}<w_{ap}$, then the defect is certainly diffuse and $w_{ap}-w_{exp}$ gives an estimate of λ, the defect diffuse length. One then obtains the real defect width $w = 2w_{ap} - w_{exp}$. Moreover, the fit of the experimental triple line front with the sharp defect leads to a value of the proportionality constant $C = w_{est}\varepsilon_{0,est}/(\pi\gamma\theta^2)$. In C, the value chosen for w_{est} is w_{ap}, the apparent width $w_{ap} = (w-\lambda)$. Thus, from the preceding discussion comparing the two theoretical triple line fronts for sharp and diffuse defect profiles, the value $\varepsilon_{0,est}$ used in C is ε_0, the value of the difference in surface free energy on the sharp part of the diffuse defect. The fit of the triple line front, under such conditions, is then equivalent to the fit of the data with the diffuse defect triple line front, with the value of $w\varepsilon_0/(\pi\gamma\theta^2)$ and a defect width w.

2.3. Comparison with the literature

Outside of the zone occupied by the defect, the triple line follows a logarithmic law in accordance with the original, simpler form (2).

For comparison within the defect zone, we have compared our analysis with the recent work of Nikolayev and Beysens [11]. They examined the dynamics of triple line deformation induced by a defect on a vertical surface. From energy minimisation principles and Fourier transform methods, they proposed an analytical expression for the triple line deformation, denoted δ_{NB}, by a stripe type defect of width w:

$$\delta_{NB}(x) = \frac{\varepsilon_0}{\pi\gamma}\left(\int_0^{w/2+x} K_0(u/l_c)du + \int_0^{w/2-x} K_0(u/l_c)du\right) \tag{16}$$

where K_0 is the modified Bessel function of zeroth order. The capillary length, l_c, appears here, as gravity is the main force that counterbalances the capillary effect. We have adapted their strategy in order to depict the triple line shape on a plane tilted at an angle α from the horizontal plane. Therefore, as stated elsewhere [9, 12, 13], the pull force is divided by θ^2 and l_c is changed into $l_c^* = l_c(\sin\alpha)^{-1/2}$ and δ_{NB} becomes δ_{NB2}, for a stripe defect of width w:

$$\delta_{NB2}(x) = \frac{\varepsilon_0}{\pi\gamma\theta^2}\left(\int_0^{w/2+x} K_0(u/l_c^*)du + \int_0^{w/2-x} K_0(u/l_c^*)du\right) \tag{17}$$

We have computed expression (17) for various values of w/l_c^* (Fig. 4) and compared $\delta_{NB2}(x)$ to $\delta(x)$ obtained from equation (11). The maximum pinning is obtained for small angles (when gravity is negligible), meaning small values of α

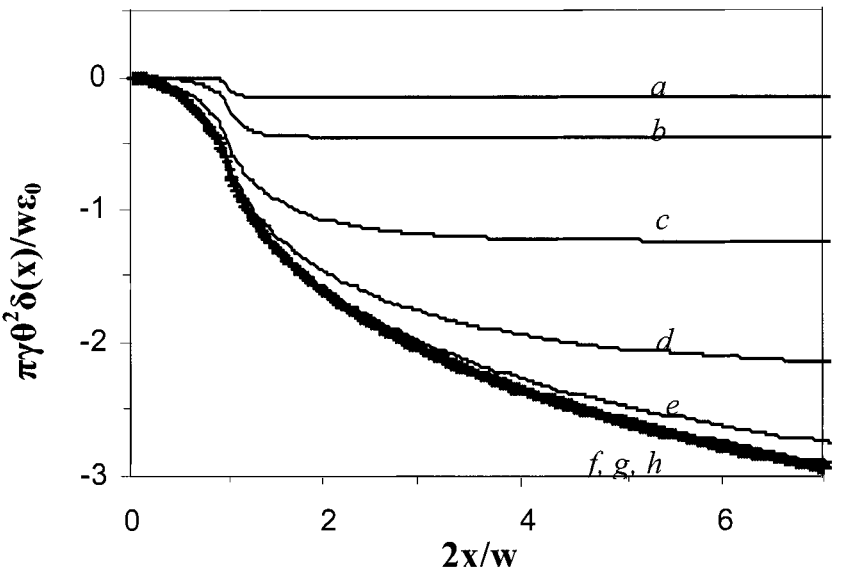

Figure 4. (a-g) Triple line front deformation by a sharp defect of width w according to equation (17) for $2l_c/w$ = (a) 0.1, (b) 0.3, (c) 1, (d) 3, (e) 10, (f) 30, (g) 100. (h) Triple line front deformation by the same defect according to equation (11).

or large values of l_c^*. Moreover, under these conditions, equation (17) is identical to equation (11).

3. EXPERIMENTAL

3.1. PTFE surface preparation

PTFE samples (Goodfellow, 2.5×1.5×0.1 cm^3) were polished with emery paper (P4000, Presi, France), rinsed in distilled water, then polished on a wet cloth (DP-Nap, Struers, France) until a shiny "mirror" surface was obtained.

Following this, a narrow band (50–200 μm) of treated material was produced by electrochemical treatment using (i) disk and (ii) band ultramicroelectrodes. In a few cases, the treatment was restricted to local circular spots.

The ultramicroelectrodes used were: (i) Pt disks made from wires of 25, 50 or 100 μm diameter embedded in an insulating glass as described previously [14], and (ii) a Au band (width 50 μm, length *ca.* 3.5 mm) microelectrode assembly as recently proposed [15]. The latter assembly consisted of a plaque of Au separated from two Pt wires embedded in epoxy. After polishing, the assembly revealed a Au band of width 50 μm and length 3.5 mm surrounded by two disks of radius 25 μm. The electrolytic solution consisted of 3 ml dimethylformamide (DMF) as the solvent, 0.1 M NBu_4BF_4 as the electrolyte and typically contained 0.05 M 2,2'-

bipyridine (M_1, E^o_{M1} = - 2.10 V *vs.* saturated calomel Electrode, SCE) and 2 mM terephthalonitrile (M_2, E^o_{M2} = - 1.51 V *vs.* SCE). The scanning electrochemical microscope (SECM) consisted of a three-stage assembly of micro-step motors driven by a controller ESP300 (Newport) piloted by a PC. The current flowing through the ultramicroelectrode was controlled by a potentiostat CHI720 (CH Instruments, USA) piloted by a PC.

It was necessary to ensure the parallelism between the PTFE surface and the (i) microelectrode disk path or (ii) the plane of the band microelectrode assembly. For this reason the electrolytic solution used contained, in a more dilute concentration, a second redox mediator, M_2 (terephthalonitrile), whose E^0_{M2} = -1.51 V *vs.* SCE is not negative enough to ensure reduction of PTFE. If the electrode is held at a potential of E = -1.60 V *vs.* SCE (enough to generate M_2 radical anion but not M_1 radical anion), the PTFE surface behaves as an insulator, i.e., moving the electrode towards the PTFE surface results in a decrease in the current.

In case (i), the PTFE and electrode surface parallelism was adjusted so that any lateral displacement of the disk electrode at a constant distance from the PTFE surface would result in a constant current. Parallelism was then obtained by mechanical adjustment of the PTFE surface plane until a constant current corresponding to d = 0.64 *a*, (where *a* is the electrode radius) was obtained during the whole lateral microelectrode displacement.

In case (ii), the parallelism between the PTFE surface and the band microelectrode assembly was adjusted by changing the inclination of the PTFE surface until the current at the two external disks microelectrodes was identical. The band microelectrode assembly was then moved toward the PTFE surface until the band current corresponded to the value expected for d = 0.64 *a* [15].

The (i) disk or (ii) band electrode was then biased at a more negative potential (E = -2.15 V *vs.* SCE) to ensure M_1 reduction into $M_1^{\bullet -}$ which, in turn, reduced the PTFE.

In case (i), local transformation of PTFE along the band was achieved when the disk microelectrode was displaced at a constant distance of d = 0.64 *a*, and at a constant speed of 5 μm/s. The band obtained was as long as the displacement and its width depended on the electrode radius, *a*, the distance between the electrode and the PTFE surface, d, and on the relative speed of the electrode. It was possible to produce bands having widths ranging from *ca.* 80 to 250 μm. Typically 0.3 to 1 mm long bands were fabricated within 60 to 200 s.

In case (ii), the PTFE was instantaneously transformed along a band of length equal to the length of the Au band. Its width was *ca.* 6 times that of the Au band for a treatment time of 150 s.

3.2. Wetting experiments

Tricresyl phosphate (TCP, Aldrich, 90%, mixture of isomers) either pure or with a 3.5 mM concentration of a fluorescent dye (Rhodamine B (RB) or Curcumine

Table 1.
Wetting data on PTFE

Test liquid	γ (mN m^{-1})	θ_r (°)	θ_a (°)	$\varepsilon_{max} = \gamma(1-\cos\theta_{r/a})$ (mJ/m^2)
TCP	40.9	55	66	17/24
TCP + Rhodamine B (RB)	41.9	51	62	15/22
TCP + Curcumine (Cur)	41.9	50	62	15/22
Water	72.6	98	108	83/95

γ is the liquid surface tension, θ_r and θ_a are the receding and advancing contact angles, respectively, of the liquid on virgin PTFE. ε_{max} is the maximum wettability difference as given by equation (3) for ε with $\cos\tilde{\theta} = 1$.

(Cur), Aldrich) in attempts to facilitate observation of the triple line, and ultrapure water (Milli-Q grade) were used as the test liquids. The liquid surface tension, γ, and the virgin PTFE wetting ability by the different mixtures used were obtained from Wilhelmy plate and contact angle measurements, respectively (see Table 1). The different values obtained and used are also given in Table 1. The column, ε_{max}, corresponds to the maximal values of ε from equation (3), as defined when $\cos\tilde{\theta} = 1$ and where θ is taken either as θ_r the receding or as θ_a the advancing angle.

Treated sheets of PTFE were mounted almost horizontally (with an angle of *ca.* 5° with respect to the horizontal) in a clamp. By means of a micro-displacement control, the PTFE sample could be immersed or emersed into or from the TCP, along the direction parallel to the treated band, in a small liquid bath. Owing to the large contact angle of water on PTFE, this procedure could not be used with water as a test liquid. In this case, a large continuous film of water was deposited with a syringe onto the tilted PTFE surface. We carefully checked that the treated band was only partially covered by the film of water and that the film was straight and perpendicular to the band 2 mm away from it. For this purpose the films used typically had dimensions of 20×10 mm^2.

The system described was placed under a vertically mounted optical microscope (magnification up to ×32) with a camera (magnification ×3, 4 Mpx resolution image), video recorder and PC set-up attached. Observation and recording of static wetting fronts corresponding to the solid/liquid/air triple line were undertaken so that the contact line shape could be analyzed and compared with theoretical predictions.

4. RESULTS AND DISCUSSION

4.1. SECM etching of PTFE

The PTFE was locally reduced to a polymeric carbon material by SECM. Figure 5 shows the schematic principle of PTFE surface reduction by SECM using both disc and band electrodes. The stable radical anion of a redox mediator, denoted $M_1^{\bullet -}$, is generated at an ultramicroelectrode biased at a potential $E < E^0_{M1}$ in the close vicinity of the PTFE surface. Typically, if the electrode, of radius (or half-width) a, is held within a distance of $2a$ from the sample surface, the radical anion generated can react with the polymer surface provided it is a strong enough reducer [16]. This reaction transforms PTFE into a polymeric carbonaceous material (black material in Fig. 5) and regenerates M_1, according to the following global equation [17]:

$$(2+\delta)n\ M_1^{\bullet -} + \delta n\ NBu_4^+ + (-CF_2-)_n \rightarrow$$
$$\rightarrow (2+\delta)n\ M_1 + ((-C^{\delta -}-)_n\ ;\ \delta n\ NBu_4^+) + 2n\ F^- \qquad (18)$$

where NBu_4^+ is the cation of the electrolyte and $((-C^{\delta -}-)_n\ ;\ \delta n\ NBu_4^+)$ represents the n-doped carbonaceous material resulting from reduction.

The amount of current flowing through the microelectrode is strictly correlated to the amount of charge used for the transformation of the PTFE material. For a stationary electrode (band or disk), a carbonaceous area, which is the image of the electrode geometry (band or disk), is imprinted on the PTFE surface. When a disk electrode was moved above the PTFE sample, a band was imprinted on the PTFE surface. In fact, the transformation of the material extends also to the bulk of the material, but at a rate much slower than the surface transformation rate. The surface reaction rate is dependent on the reaction time and also on the disk scan rate.

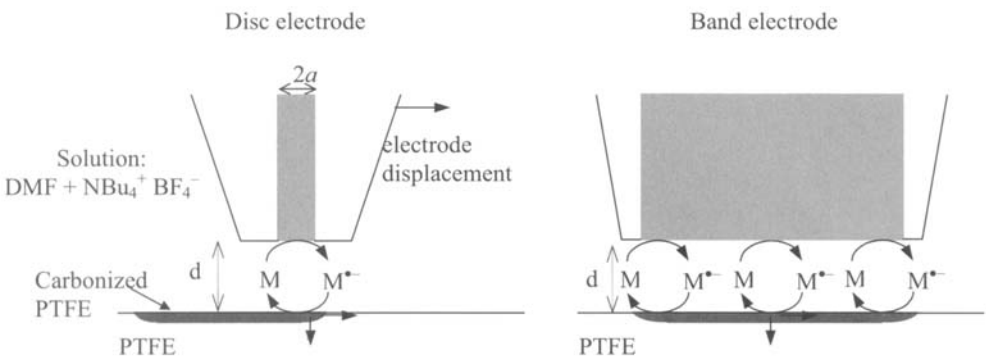

Figure 5. Schematic representation of the PTFE surface treatment by SECM with a disc (left) or a band (right) electrode.

In the time region used for the PTFE band etching, if we assumed the expansion of the band etching as diffusion-like, we may estimate the length, λ, of the transformation diffuse layers, located at each border of the band. In this diffuse area the PTFE transformation is likely only partial, and we obtain the electrode current i:

$$i \approx nFD_S \frac{C_P}{\lambda_r} rh \tag{19}$$

where F is the Faraday constant, D_S is the diffusion rate of the reducing species for surface carbonization, C_P is the concentration of the monomer unit in the polymer ($C_P = 22$ mol·l^{-1}) and n the number of electrons exchanged for reduction of each monomer unit ($n = 2+\delta = 3$), λ_r is the length of the reducing species diffusion layer along the surface in the carbonized region, r is the surface etching propagation length ($r \approx w/2$) and h is its bulk propagation length. The bulk propagation is diffusion-like and $h = (D_b t)^{1/2}$ with $D_b \sim 10^{-11}$ cm^2·s^{-1} and t is the time required for the PTFE etching.

The propagation of the carbonization at the material surface is typically 100-times faster than that in the bulk; thus, $D_S^{1/2} \sim 100\ D_b^{1/2}$, which leads to $D_S \sim 10^{-7}$ cm^2·s^{-1}. Typically, the etching of a band of width $w = 80$ μm was achieved with an electrode of radius $a = 12.5$ μm moved at $v = 5$ μm/s with a current of 2×10^{-7}A. The electrode might be assumed to be a discoid source of etchant whose diameter is about twice larger than that of the electrode and the band etching occurs during a time-of-flight $t \sim 4a/v = 10$ s. A value of $\lambda_r \sim 2$ μm then ensues. Even for the smallest carbonaceous band ($w = 80$ μm) the reaction layer represents less than 5% of the apparent black part of the transformed band. Therefore, to a first approximation, it is not worth using the trapezoidal-profile model and the defect may be considered as sharply defined.

It is difficult to estimate the surface free energy (dispersion and non-dispersion components) for an entire PTFE surface treated under the same conditions, due to the heterogeneity of the treatment on large surfaces. However, the values of the surface free energy of PTFE modified under strongly reducing conditions are reported to be in the range 40–50 mJ/m^2 [18–20]. This large increase in the surface free energy is mainly due to the oxidation of the carbonaceous material by air or water. It tends to oxygenate the surface and then to increase the hydrophilicity of the treated band compared to original PTFE.

With TCP as a wetting liquid, quasi-total or total wetting is expected with γ_{SV}-γ_{SL} of the order of γ, leading to values of the excess surface free energy ε_0 of about 20 mJ/m^2. If water is the wetting liquid, the wetting is partial and a receding contact angle of about 60° is expected on the etched band and, consequently, the expected excess surface free energy ε_0 is about 40 mJ/m^2.

4.2. *Triple line front analysis*

Figure 6 represents typical experimental triple line fronts obtained on an etched band of width 80 μm with TCP and water as test liquids. After digitization, the images were used in conjunction with regression analysis and equation (11) to obtain the best fits as shown in Fig. 6a and 6b, respectively, for the wetting by TCP and water of the same etched band. As stated in our earlier work [7] with TCP, the whole wetting profile fitted well to equations (2) and (11) outside the defect. Equation (11) also correlated successfully with the wetting profile inside the defect. Both the experimental and theoretical profiles demonstrate the transition from a concave triple line outside the "defect" to a convex triple line within the

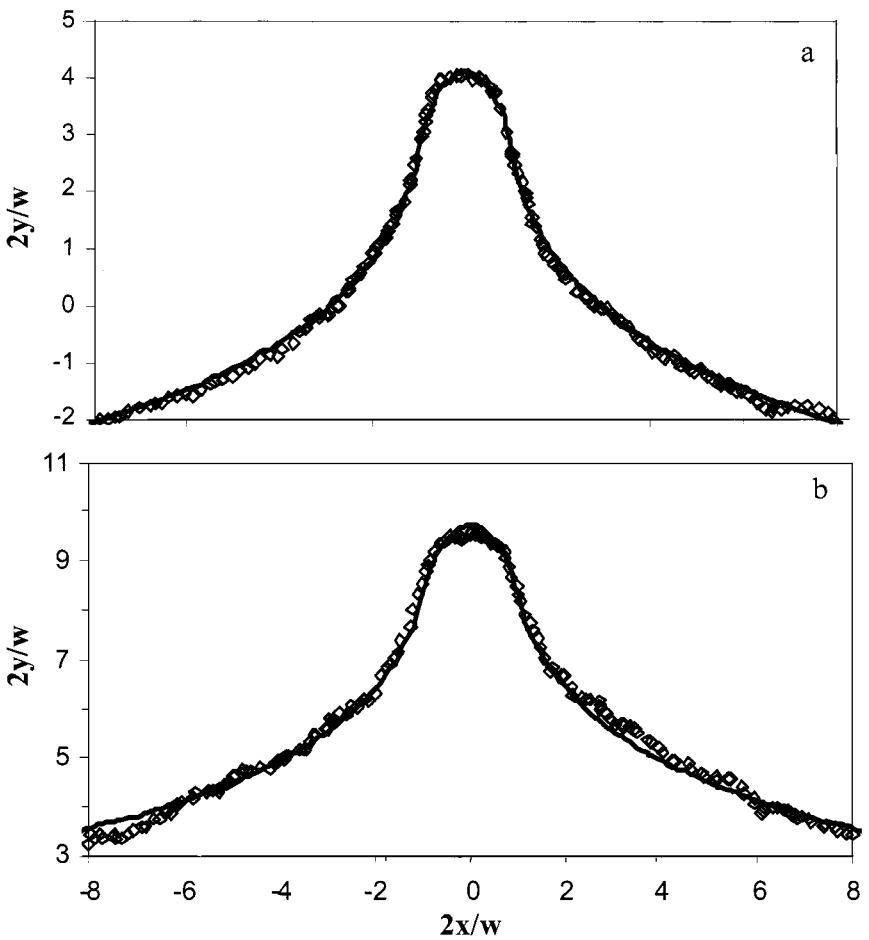

Figure 6. (a) (–) Experimentally observed TCP triple line front deformation by a 80 μm wide etched PTFE band. (◊) Best fit of the triple line front by equation (11). (b) (–) Experimentally observed water triple line front deformation by a 80 μm wide etched PTFE band. (◊) Best fit of the triple line front by equation (11).

confines of the heterogeneity. The inflexion points of the triple line correspond to the borders of the heterogeneity. The apparent width, w_{ap}, of the defect is obtained from the second derivative of the triple line front. It is then compared to the width of the black etched material, w_{exp} = 80 μm. We find $w_{exp} = w_{ap}$ to within 5%, which indicates that if the defect is diffuse λ is lower than 2 μm in agreement with its proposed estimate.

Thus, the regression fits allowed us to calculate the values of ε_0, the "excess wettability", from equation (11) either using w_{ap} and ε_0, or from equation (2) with $f = \varepsilon_0 w_{ap}$; both approaches give the same results.

A summary of the principal experimental findings from these wetting experiments on etched PTFE (w = 80 or 290 μm) is presented with those previously obtained [7] in Table 2. With TCP as test liquid, we obtained a value of $\varepsilon_0 = 47 \pm 6$ mJ/m^2 in good agreement with those already reported. Again, the actual values of ε_0 are considerably higher than the maximum theoretical value given by $\varepsilon_{max} = \gamma (1 - \cos\theta) = 17$ mJ/m^2 taking the highest possible value of $\cos\tilde{\theta}$, i.e. unity. The situation thus corresponds to total wetting of the etched material with a contact angle of zero. Owing to the high surface energy value of the reduced PTFE, a complete wetting is likely. The excess surface free energy of *ca.* 30 mJ/m^2 could characterize the pinning force due to the spreading of TCP on the etched band. Indeed from time to time, thin isolated droplets of TCP were observed on the dewetted parts of the etched PTFE band. The possible role of the liquid spreading on the triple line profile has not been studied so far, and we are currently investigating it from both theoretical and experimental viewpoints.

The case of water as test liquid is also critical. Indeed, the value of $\varepsilon_0 = 105 \pm 5$ mJ/m^2 deduced from equation (11) is again higher than the maximum theoretical value, ε_{max} = 83 mJ/m^2. However, a complete wetting of the etched band is less likely than that for reduced PTFE. Indeed, after the whole PTFE surface was reduced by dipping into a reductive solution, water droplets were shown to spread

Table 2.
Summary of principal wetting experiments performed with TCP and water on etched PTFE

Geometry of treated zone (width in μm)	Liquid	Irradiation time in visible light (h)	Number of experiments	ε_0 (mJ/m^2)
Band (80, 120, 180, 200, 220, 290)	TCP/RB/Cur	<1[a]	18	47 ± 6
Band (180)	RB	1	1	34
Band (180)	TCP/Cur	>4	5	20 ± 2
Band (80)	Water	<1[a]	3	105 / 34[b]

Variability of band width was typically ± 5 μm. The wetting triple line was observed in the static receding mode. The parameter ε_0 corresponds to "excess wettability" as defined by equation (7). Values for band widths 80 < w < 290 μm are from Ref. [7].

[a]Low intensity irradiation.

[b]Second value obtained when using $\sin^2\theta$ instead of θ^2 in (11).

more easily on the reduced surface and a receding contact angle of about 60° was observed [18, 19]. The overestimate of ε_0 might be due to the assumptions made during the calculation of the triple line front. Indeed, water is a non-wetting liquid for virgin PTFE and the receding contact angle is greater than 90°: this contradicts the assumption of small values of θ. This argument has already been mentioned from a theoretical point of view [21]. The variation of the liquid–vapor interfacial energy due to the deformation of the surface of the liquid was originally estimated for small angles [2]. It was generalized to arbitrary values of θ [21], and consists, for geometrical reasons, in substituting θ^2 by $\sin^2\theta$ in the expression for the capillary energy and, thus, leads to the same substitution in equation (2). Similarly, in the methodology we have adopted [6], we have used the same substitution, since the approximation of small angles comes mainly from the relation between the axisymmetric droplet contact radius, r_0, and its curvature radius, $R = r_0/\sin\theta \sim r_0/\theta$. However, the experimental work demonstrated the validity of the use of θ^2 when a drop of a non-wetting liquid was placed on a periodic array of square hydrophilic defects patterned on a hydrophobic surface [22].

Consideration of more general values of θ in the establishment of equation (11) also leads to the replacement of θ^2 by $\sin^2\theta$. A much lower value of $\varepsilon_0 = 34 \pm 4$ mJ/m^2 is obtained when taking into account this $\sin^2\theta$ term. A contact angle of 70 ± 5° then ensues for water on the reduced PTFE, in better agreement with the estimated value of 60°. The same consideration with TCP slightly modified the excess surface free energy (40 mJ/m^2 instead of 50) and, therefore, does not change our discussion on excess wettability.

5. CONCLUSIONS

This paper links the electrochemical modification of initially low surface free energy polymers and the wetting theory. Earlier predictions suggested that the general form of an initially straight wetting triple line perturbed by a local (high surface energy) "defect" should be logarithmically decaying outside of the "defect". This concave wetting line should present an inflexion point at the (assumed) sharp barrier between the defect and the homogeneous material on each side, and then a change to convexity should ensue within the defect. By using microelectrodes, "defect" dimensions (of the order of tens of μm) suitable for wetting studies can be produced on polymer surfaces.

It has been found that the wetting behavior is certainly qualitatively in agreement with theoretical predictions: good fits between theoretical equations and observed wetting fronts have been found. The theory assumes sharp cut-offs between the defect and surrounding material. Modifying the theory, allowing for diffuse boundaries, extends it to a more precise description of heterogeneous surfaces obtained by chemical means. A special feature of the theoretical treatment is

a quantity which we term "excess wettability" and that estimates of this quantity were made and found sometimes to be too high.

By allowing for some corrections in the treatment of wetting, specifically by no longer assuming small contact angles, an improved correlation between experiment and theory has been obtained.

REFERENCES

1. D. Mandler, in: *Scanning Electrochemical Microscopy*, A. J. Bard and M.V. Mirkin (Eds.), p. 593. Marcel Dekker, New York, NY (2001).
2. J. F. Joanny and P. G. de Gennes, *J. Chem. Phys.* **81**, 552 (1984).
3. P. G. de Gennes, *Rev. Mod. Phys.* **57**, 827 (1985).
4. Y. Pomeau and J. Vannimenus, *J. Colloid Interface Sci.* **104**, 477 (1985).
5. L. W. Schwartz and S. Garoff, *J. Colloid Interface Sci.* **106**, 422 (1985).
6. M. E. R. Shanahan, *J. Phys. D: Appl. Phys.* **22**, 1128 (1989).
7. F. Kanoufi, C. Combellas and M. E. R. Shanahan, *Langmuir* **19**, 6711 (2003).
8. T. Young, *Phil. Trans. Roy. Soc. (London)* **95**, 65 (1805).
9. G. D. Nadkarni and S. Garoff, *Europhys. Lett.* **20**, 523 (1992).
10. M. E. R. Shanahan, *Colloids Surfaces A* **156**, 71 (1999).
11. V. S. Nikolayev and D. A. Beysens, *Europhys. Lett.* **64**, 763 (2003).
12. J. A. Marsh and A. M. Cazabat, *Phys. Rev. Lett.* **71**, 2433 (1993).
13. J. F. Joanny and M. O. Robbins, *J. Chem. Phys.* **92**, 3206 (1990).
14. A. J. Bard, F. R. F. Fan and M. V. Mirkin, in: *Electroanalytical Chemistry*, A. J. Bard (Ed.), Vol. 18, p. 243. Marcel Dekker, New York, NY (1994).
15. C. Combellas, A. Fuchs and F. Kanoufi, *Anal. Chem.* **76**, 3612 (2004).
16. C. Combellas, J. Ghilane, F. Kanoufi and D. Mazouzi, *J. Phys. Chem. B* **108**, 6391 (2004).
17. C. Amatore, C. Combellas, F. Kanoufi, C. Sella, A. Thiébault and L. Thouin, *Chem. Eur. J.* **6**, 820 (2000).
18. K. Brace, C. Combellas, M. Delamar, A. Fritsch, F. Kanoufi, M. E. R. Shanahan and A. Thiébault, *J. Chem. Soc. Chem. Commun.*, 403 (1996).
19. K. Brace, C. Combellas, E. Dujardin, A. Thiébault, M. Delamar, F. Kanoufi and M. E. R. Shanahan, *Polymer* **38**, 3295 (1997).
20. L. Kavan, *Chem. Rev.* **97**, 3061 (1997).
21. M. O. Robbins and J. F. Joanny, *Europhys. Lett.* **3**, 729 (1987).
22. G. Wiegand, T. Jaworek, G. Wegner and E. Sackmann, *J. Colloid Interface Sci.* **196**, 299 (1997).